Received: 21 February 2023 | Revised: 4 December 2023 | Accepted: 12 December 2023

DOI: 10.1002/rcs.2615

ORIGINAL ARTICLE

The International Journal of Medical Robotics and Computer Assisted Surgery

WILEY

Robotic-assisted burring in total hip replacement: A new surgical technique to optimise acetabular preparation

Tiancheng Li[1] | Peter Walker[2] | Richardo Khonasty[1] | Victor A. van de Graaf[2] | Eric Yelf[2] | Liang Zhao[1] | Shoudong Huang[1]

[1]Robotics Institute, Faculty of Engineering and Information Technology, University of Technology Sydney (UTS), Sydney, New South Wales, Australia

[2]Concord Repatriation General Hospital, Concord, New South Wales, Australia

Correspondence

Tiancheng Li, Robotics Institute, Faculty of Engineering and Information Technology, University of Technology Sydney (UTS), Sydney, NSW, Australia.
Email: Tiancheng.Li-1@student.uts.edu.au

Funding information

PMSW Research Pty Ltd, Australia

Abstract

Background: In Total Hip replacement (THR) surgery, a critical step is to cut an accurate hemisphere into the acetabulum so that the component can be fitted accurately and obtain early stability. This study aims to determine whether burring rather than reaming the acetabulum can achieve greater accuracy in the creation of this hemisphere.

Methods: A preliminary robotic system was developed to demonstrate the feasibility of burring the acetabulum using the Universal Robot (UR10). The study will describe mechanical design, robot trajectory optimisation, control algorithm development, and results from phantom experiments compared with both robotic reaming and conventional reaming. The system was also tested in a cadaver experiment.

Results: The proposed robotic burring system can produce a surface in 2 min with an average error of 0.1 and 0.18 mm, when cutting polyurethane bone block #15 and #30, respectively. The performance was better than robotic reaming and conventional hand reaming.

Conclusion: The proposed robotic burring system outperformed robotic and conventional reaming methods to produce an accurate acetabular cavity. The findings show the potential usage of a robotic-assisted burring in THR for acetabular preparation.

KEYWORDS

acetabular preparation, robotic-assisted surgery, THR, UR10 robot

1 | INTRODUCTION

Osteoarthritis constitutes a major musculoskeletal burden for elderly people worldwide, reflected by being ranked as the 11th highest contributor to global disability.[1] Total Hip replacement (THR) (Figure 1) is the effective intervention once conservative therapies have been exhausted. The number of THR required is increasing significantly due to ageing of the population.[2,3]

A critical step in THR is to precisely cut an accurate and smooth hemisphere into the socket of the hip bone (acetabulum) such that the press-fit acetabular component can be well secured and fitted. The exact press fit of the components allows initial stability to be

FIGURE 1 Left: Hip anatomy (image from the American Academy of Orthopaedic Surgeons); Middle: Osteoarthritis; Right: Total hip replacement (THR).

obtained and is essential for bony ingrowth.[4,5] Underreaming may result in failure for the component to be appropriately seated or periprosthetic fracture.[6] Overreaming can lead to micromotion and failure to achieve bony ingrowth. Inappropriate positioning of the acetabular cup can lead to impingement or THR dislocation.[7,8]

Reaming has traditionally been performed by hand hand-held power reamer (Figure 2). However, over recent years, robotic-assisted reaming techniques are gaining popularity to optimise the cup position and therefore the surgical outcome.[9] The proposed advantages of using robotic techniques in THR are minimising surgical errors and improving implant position accuracy, thereby reducing the incidence of dislocation.[10,11] Bone stock may also be preserved in robotic-assisted THR compared with conventional THR by using femoral head size as an approximate surrogate measure of acetabular bone resection.[12] Robotic and navigation-guided techniques have been shown to be more consistent than other techniques in placing the acetabular component into Lewinnek's safe zone.[13,14]

The Mako robotic arm (Stryker)[15] is currently the most commonly used robotic system for THR which is significantly advanced over earlier robotic systems[16] such as Robodoc.[17] The high financial cost of the system, however, makes its widespread use prohibitive. Alternatively, a low-cost robotic system based on the UR10 collaborative robotic arm (Universal Robots) equipped with a reamer has been studied with bone block models, demonstrating a higher accuracy of robotic-assisted reaming as compared to reaming by hand.[18] Reamers (Figure 2) may be prone to generate excessive heat leading to osteonecrosis due to the large cutting contact area, and may lead to aseptic loosening.[19] Further potential disadvantages of reamers can only create symmetrical shapes, so it may be inconvenient for acetabular defect or augment. Burring is an alternative and is used in robotic-assisted systems for total knee replacement but its use in THR for acetabular resection is yet to be realised.[20]

Therefore, this research studies the feasibility of using a burring device to cut a hemisphere for acetabular preparation during THR. We propose a robotic burring system using a burr head attached to a UR10 robot. We will describe the development of a robotic system, the trajectory design, and compare the performance of the proposed system to both robotic reaming and conventional reaming. The key

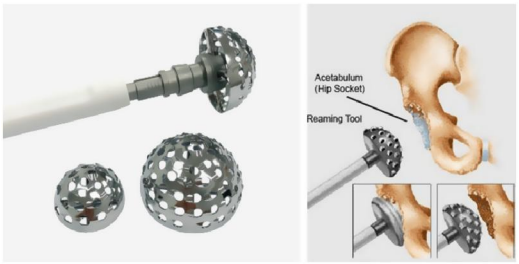

FIGURE 2 Left: Acetabular reamer for Total Hip replacement (THR); Right: Illustrating how reaming is done.

advantages of this method include: (i) the more accurate and smoother cut surface can be created, which can enhance the contact area of the acetabular cup with the bone, thus reducing the chance of loosening; (ii) a robotics system which provides not only acetabular cutting control but also includes a registration programme and safety settings for easy clinical integration; (iii) an end-effector design offers the potential for the application of a minimally invasive and innovative superior-based muscle-sparing THR technique.

2 | METHODOLOGY

2.1 | Robotic burring system design

The robotic burring system is composed of a 6 degree of freedom rigid link positioning collaborative manipulator, a burr head, a spindle, a C-arm, and a sterile offset separating the robot with the C-arm (Figure 3). The core control algorithm includes position control, velocity control, and admittance control.

2.1.1 | Collaborative manipulator and C-arm

At the core of the system is a UR10 collaborative manipulator made by Universal Robots. The main factors in choosing the UR10 are its board ranges of use, its economics, the safety of physical human-

robot interaction, and the emergency stop when the velocity or force encountered by the robot exceeds a certain threshold. As shown in Figure 3, the modification of the end-effector mounting mechanism to a C-arm not only allows for its use with any current hip approach such as the most common posterior approach[21] but also offers the potential for the application of a minimally invasive and innovative superior-based muscle-sparing THR technique[22] (Figure 4). In this minimally invasive approach, a 5 mm hole is drilled into the lateral femoral cortex, after which a broach handle is attached to the broach via a rod, aligning it with the drill hole with options for different femoral neck angles (e.g. 135 or 128°). Next, a burr typically 12 mm in diameter is attached to a thread on the end of the rod and the robot will move the C-arm in a circular motion to prepare the acetabulum to the correct size and position.

Since the rod goes through a hole in the broach, the bone is protected from any damage. The advantages of this technique are that the surgery can be performed without retraction of the femur, and fewer soft tissue releases are required. This burring, however, could also be performed using any conventional hip approach allowing for a direct line of sight for the robot to the acetabulum. Currently, a sterile offset attachment has been designed to maintain a safe distance between the C-arm and the robot end-effector. This structure can also ensure that the surgical field remains sterile.

2.1.2 | Patient and surgeon safety

A critical requirement of any collaborative robot system is maintaining the safety of the human operator. This facet was considered in all the design aspects of the robotic burring system. The UR10[23] is a collaborative robot designed to meet standards regarding physical human-robot interaction. The operating range of UR10 is 1.3 m, which is larger than most similar collaborative robots. Therefore, it can provide a larger operating space for surgeons. As the robotic burring system is to be used in THR, ensuring the safety of patients is of paramount importance. During the acetabular burring process, the force and depth of reaming exerted by the burr head on the patient's bone are monitored. If any predefined settings are exceeded or the burr moves out of its predefined path the robot will automatically turn off.

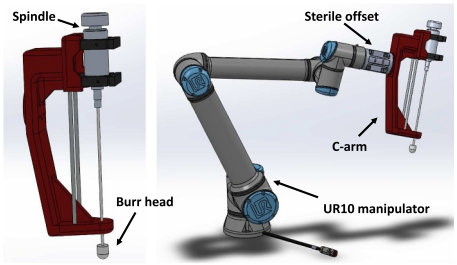

FIGURE 3 Left: The C-arm for robotic burring system; Right: The structure of the robot burring system with the sterile offset and the C-arm.

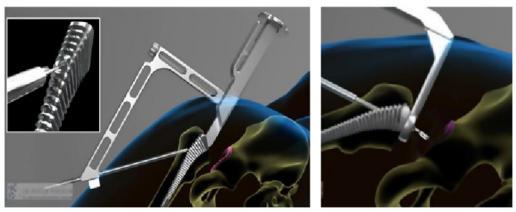

FIGURE 4 Superior-based muscle-sparing Total Hip replacement (THR) approach with a 5 mm transfemoral drill hole: Left: a drill hole made in lateral femoral cortex using a special guide; Right: a rod is passed through the C-arm into the broach, attaching the burr at the end.

2.1.3 | Admittance control for registration

Prior to the burring, the acetabular landmarks and the centre of rotation need to be identified. The registration is then matched to the preoperative plan typically from a 3D computed tomography scan. The patient-specific 3D printed tool (Figure 5) is fitted within the acetabulum to the appropriate orientation and the rod is guided into a hole in this tool. This hole orientates the C-arm and rod as well as predetermines the centre of rotation. During the surgery, the registration tool is mounted on the end of the C-arm and placed into the patient's acetabular socket. The registration plane (the orange shaded surface in Figure 5 Right) is then set and is the same as the eventual burring plane, consistent with the preoperative planning of the acetabular cup positioning.[24] The robotic system then records the centre position (the starting point of the cutting trajectory) and the cutting direction. The process of controlling the smooth movement of the robot end-effector and the accurate placement of the registering tool can be realised with admittance control.[25] If force $\mathbf{F}$ represents the surgeon's intention, multiplied by the admittance matrix K, the Cartesian velocity command can be generated as $\dot{\mathbf{X}} = K \cdot \mathbf{F}$. The Cartesian velocities are transformed to joint velocities $\boldsymbol{\theta}$ using the inverse Jacobian matrix, which are then sent to the Universal Robot controller as joint velocity commands. A slower speed was used in order to achieve more control when locating the acetabulum resulting in increased accuracy.

2.1.4 | Position control for cutting process

A position control algorithm[26] is applied on the UR10 robot to realise autonomous cutting. This algorithm specifies the global positions and

FIGURE 5 Registration: the tool is determined by segmenting the preoperative patient-specific pelvic fossa with a 3D computed tomography (CT) scan and the orange shaded surface is the same as the eventual burring plane.

trajectory for the robot end-effector such that the burr head attached to the end-effector can cut the planned shape. The relative position between the burr head and the robot end-effector is accurately calibrated based on the computer-aided designs, so that the proposed trajectory of the robot end-effector correctly resects the required hemisphere. The details of the trajectory design are given in the following section.

2.2 | The robot trajectory optimisation

The method that automatically generates the 3-Dimensional (3D) trajectory for a given size of a hemisphere is developed for the position control. The objective was to optimise the trajectory such that the burr head followed while fast-rotating in order to cut a smooth hemisphere. Since the burr head is always perpendicular to the top round surface of the hemisphere, the angle of the hemisphere can be determined according to the direction of the burr head for realistic scenarios. Thus, without loss of generality, the trajectory is designed for cutting a hemisphere in a vertical direction. Therefore, the burr head has to make a complete circular trajectory of a certain radius in the horizontal plane, before moving down a certain distance and repeat this for the next radius. The burr head moves from one layer to the next until a complete hemisphere is formed (Figure 6).

In this situation, the 3D trajectory planning problem has been transformed into a planning problem in 2D, which is how to determine the radius of each layer of a circular trajectory and the distance of movement to the next layer. Suppose N is the number of layers of the complete cutting trajectory, and r is the radius of the target hemisphere. As shown in Figure 7, the ordinates of each layer of the burr head are divided into N equal parts according to the polar coordinate system. Therefore, the adjacent angles are equal. Then the cutting depth of the ith layer is:

$$D_i = \sin\left(\frac{\frac{\pi}{2}(i-1)}{N-1}\right) r \tag{1}$$

where $i = 1, 2, 3, \ldots, N$. Next, the radius corresponding to each layer of circular trajectory needs to be calculated.

There is a wide variety of cutting instruments that can be used for bony resections in orthopaedic surgery.[27] A cylinder burr bit with spherical head made of medical grade American Iron and Steel Institute 316L stainless steel was chosen for this application (Figure 8). The outer contour of the bur can be represented by a piece-wise function composed of two straight lines and a semicircle. Figure 9 illustrates a 2D view of using a spherical burr to cut the hemisphere, the diameter of the burr head is a and the length is b. Assume that the mathematical equation of the outer boundary of the burr head on the ith layer is $x = f_i(y)$, $i = 1, 2, 3, \ldots, N$. The mathematical model of f_i for the ith layer is related to the cutting depth D_i and circle radius of the layer R_i. Since only the outermost contour is touching surface in the actual cutting process, the mathematical model of f_i can be written as

$$x = f_i(y) = \begin{cases} R_i + \frac{a}{2}, & \frac{a}{2} - D_i < y < b - D_i \\ R_i + \sqrt{\left(\frac{a}{2}\right)^2 - \left(\frac{a}{2} - D_i - y\right)^2}, & -D_i < y < \frac{a}{2} - D_i \end{cases} \tag{2}$$

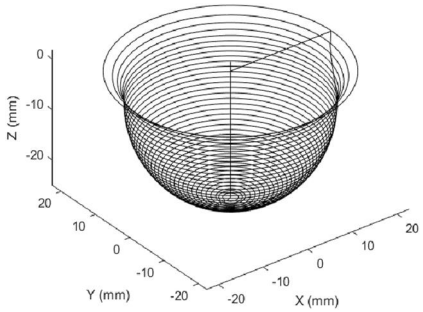

FIGURE 6 3D trajectory of the burr head.

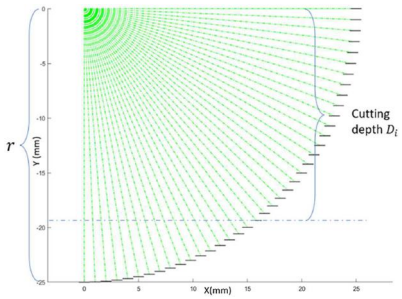

FIGURE 7 The black lines show the corresponding depth of the cut for each layer. The depth values are obtained by dividing the area equally in the polar coordinate system.

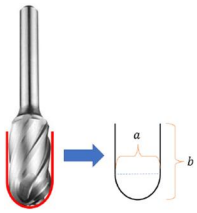

FIGURE 8 The outer contours of the spherical burr head.

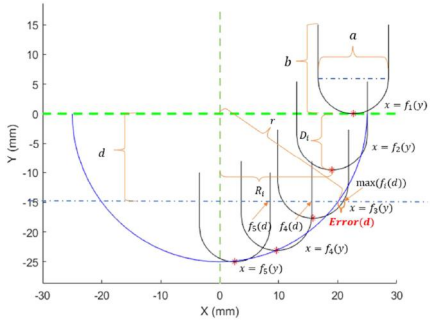

FIGURE 9 An illustration of the trajectory optimisation problem.

In Equation (2), D_i can be calculated by Equation (1) and R_i is the decision variable of the optimisation problem. As shown in Figure 9, the number of layers is selected as $N = 5$ to illustrate the optimisation problem clearly. Then for any given depth d, the ideal case is the largest outermost contour coincides the circle with radius r, so the error can be written as

$$Error(d) = \max_i(f_i(d)) - \sqrt{r^2 - d^2} \tag{3}$$

where $f_i(d)$ can be calculated by Equation (2). The following objective function is thus minimised to find the optimal R_1, R_2, ..., R_N.

$$F(R_1, R_2, ..., R_N) = \sum_{k=1}^{m} (Error(d_k))^2 \tag{4}$$

where m is the number of depths used for computing the total error. As m increases, both the accuracy of the optimised results and the calculation cost will increase. As shown in Figure 10, we selected $m = 10\,000$ in our case since the error of optimisation is almost zero and hardly decreases anymore if m increases further. Figure 11 demonstrates the final solution of the optimisation problem by Matlab.

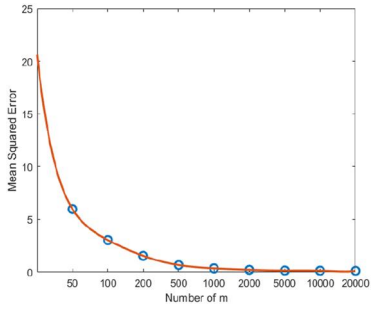

FIGURE 10 The effect of m on the optimisation results, where m is the number of depths used for computing the total error in Equation (4). The mean squared error is calculated by $F(R_1, R_2, ..., R_N)/m$.

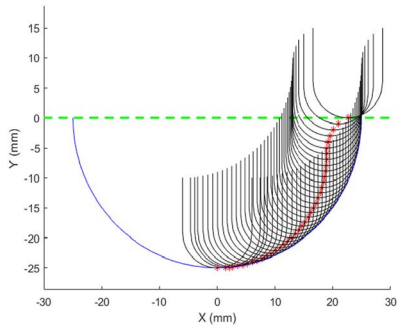

FIGURE 11 Longitudinal section of the trajectory through the centre of the target hemisphere. The black curve is the outer contour of the burr head in each layer. The abscissa represents the radius of the trajectory of the layer, and the ordinate reflects the depth information of the cutting on this layer. The red dots are the positions of the top of the burr head on each layer.

3 | EXPERIMENTS AND RESULTS

3.1 | Phantom experiments and data analysis

In order to evaluate the performance of the robotic burring system under realistic scenarios, a series of phantom experiments were performed. The experimental setup is shown in Figure 12. Foam blocks[28,29] (Pacific Research Laboratories, INC) conforming to the American Society for Testing and Materials F1839-08 Standard Specification for Rigid Polyurethane Foam[30] were selected as they allowed for a reproducible test substrate, are of uniform density, can be recycled and easily scanned. Two different densities were used. Bone block #30 has a density of 30 *pcf* or 0.80 g/cc which is similar to the normal pelvic bone. Bone block #15 has a density of 15 *pcf* or 0.24 g/cc which is used to represent the osteoporotic bone. The hemispheres were scanned using Solutionix C500, a structured light 3D scanner with absolute high accuracy up to +/−10 microns according to German Standard VDI/VDE 2634, which allows quantitative comparisons of cutting accuracy. All p-values were two tailed and no corrections were made for multiple comparisons. The statistical analysis was performed using SPSS (IBM Corp.) with significance set at 0.05. Some examples of the cut bone blocks and their 3D scans are shown in Figure 13.

The aim of the acetabular preparation based on robotic burring is to produce the cut surface which matches the hemisphere as accurately as possible. The point cloud generated by the scanner can be used to fit a sphere with a radius that is the same as the objective hemisphere. Then the fitted centre of the cut surface can be obtained. Finally, the differences between the distances from the point cloud to the fitting centre and the objective radius were used to evaluate the accuracy. Assume that the centre of cut surface is $\mathbf{C} = [C_x, C_y, C_z]^T$, and $[x_i, y_i, z_i]^T$ are the coordinate of the ith point on the surface. Then the distance from the ith point to the fitting centre can be calculated as

$$L_i = \sqrt{(C_x - x_i)^2 + (C_y - y_i)^2 + (C_z - z_i)^2}. \tag{5}$$

Suppose the radius of objective hemisphere is r_o, then $\mathbf{C}$ could be obtained by solving the optimisation problem:

$$\arg\min_{C_x, C_y, C_z} G(C_x, C_y, C_z) = \sum_{i=1}^{M} (L_i - r_o)^2 \tag{6}$$

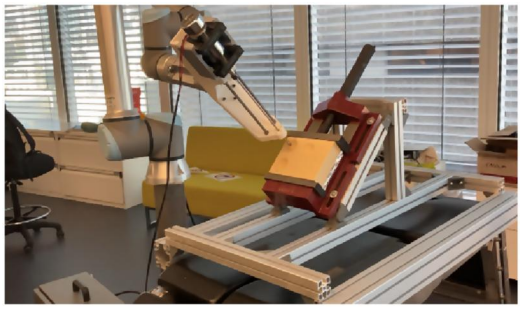

FIGURE 12 The experimental setup of robotic burring system.

where M is the number of points on the cut surface. Then the error of the ith point can be defined by

$$E_i = \|L_i - r_o\|. \quad (7)$$

Based on Equation (7), the average error of each trial can be obtained.

To obtain the relative optimal parameters of the robotic burring system, the specific experimental designs are as follows. For each setup in the tables, the cutting diameters tested ranged from 48 mm through 54 mm in 2 mm increments based on the most commonly used sized acetabular shell components in THR. The experiment was performed 3 times for each cutting diameter with robotic burring. The average quantitative error results (9 trials in total for each setup) and corresponding standard deviation, which are based on all replicate experiments for different cutting diameters under the same parameter setup of the robotic burring system, can be found in Tables 1–3.

- **Trajectory test**: the feed rate was kept constant at 15 mm/s to cut the bone block with the density of #30, and the only variable is the number of layers of the motion trajectory (80, 60, 40, 30, 20). This is for evaluating the accuracy versus the number of layers (which is closely related to the cutting time). As shown in Table 1, as the number of trajectory layers reduces, the time used for cutting decreases accordingly, while the error of the cutting surface increases. When the number of layers is reduced from 40 to 30, the error increases sharply and the decrease in time slows down. Therefore, we believe that from the parameters tested, the 40-layer trajectory is the most suited one and the following experiments were performed using this trajectory.
- **Feed rate test**: the trajectory was kept constant (the number of layers is fixed at 40) and different feed rates (15, 20, 30, 50, 75 (mm/s)) were used to cut bone blocks with the density of #15 and #30. Table 2 shows that the increasing feed rate will also increase the error. According to the experiment, 30 mm/s feed rate is the most stable setting that can produce a surface with an average error of 0.1 mm in 2 min when cutting a bone block whose density is #15. If the density of bone block is #30, the average error will be 0.18 mm.
- **Tool diameter test**: three different burr diameters were tested (12, 15, 20 (mm)). Table 3 demonstrates that a 12 mm burr diameter provided the most optimal results.

In summary, we finally selected the 12 mm burr with a 40-layer trajectory using a 30 mm/s feed rate for the robotic burring system. The test results are Exp 8 and Exp 11 for the bone block #15 and #30, respectively. To compare different categories of cutting methods, the experiments were repeated for both robotic reaming[18] and conventional (manual) reaming. The cutting diameters also ranged from 48 mm through 54 mm in 2 mm increments and were performed 3 times per cutting diameter. The results (Table 4 and Figure 14) demonstrate that the proposed robotic burring system can produce a surface with an average error of 0.1 and 0.18 mm, when cutting a bone block whose density is #15 and #30 respectively in

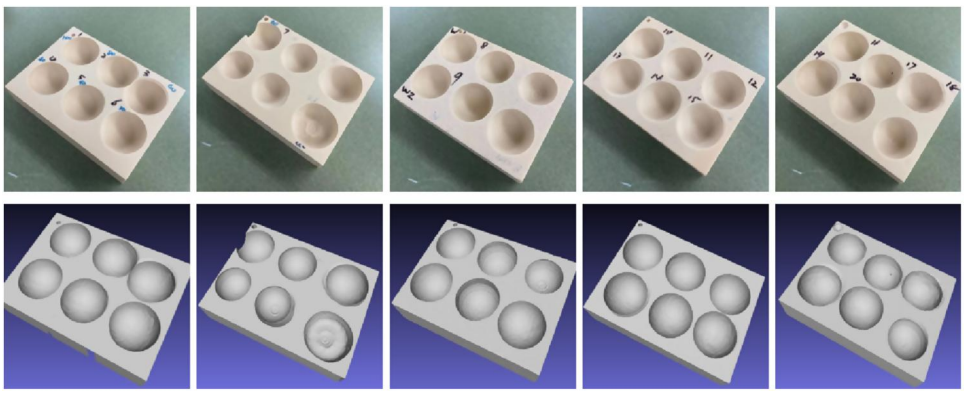

FIGURE 13 Examples of hemisphere cuts from the bone block and the corresponding 3D scan of the results for quantitative comparison.

TABLE 1 Trajectory test and results.

Setup	Density	Exp type	Feed rate [mm/s]	Number of layers	Burring bit diameter [mm]	Time cost [min]	Average error [mm]	Standard deviation
1	#30	Layer	15	80	12	7.5	0.17	0.0125
2	#30	Layer	15	60	12	5.6	0.18	0.0132
3	#30	Layer	15	**40**	12	3.8	**0.18**	**0.0131**
4	#30	Layer	15	30	12	2.9	0.22	0.0143
5	#30	Layer	15	20	12	2.0	0.23	0.0171

Note: The values in bold are to highlight the performance of the optimal or most appropriate parameter for each experimental setup.

TABLE 2 Feed rate test and results.

Setup	Density	Exp type	Feed rate [mm/s]	Number of layers	Burring bit diameter [mm]	Time cost [min]	Average error [mm]	Standard deviation
6	#15	Feed rate	15	40	12	3.8	0.07	0.0124
7	#15	Feed rate	20	40	12	2.8	0.10	0.0140
8	#15	Feed rate	**30**	40	12	1.8	**0.10**	**0.0134**
9	#15	Feed rate	50	40	12	1.17	0.12	0.0126
10	#15	Feed rate	75	40	12	0.75	0.14	0.0151
3	#30	Feed rate	15	40	12	3.8	0.18	0.0131
11	#30	Feed rate	**30**	40	12	1.8	**0.19**	**0.0114**
12	#30	Feed rate	75	40	12	0.75	0.20	0.0137

Note: The values in bold are to highlight the performance of the optimal or most appropriate parameter for each experimental setup.

TABLE 3 Tool diameter test and results.

Setup	Density	Exp type	Feed rate [mm/s]	Number of layers	Burring bit diameter [mm]	Time cost [min]	Average error [mm]	Standard deviation
11	#30	Diameter	30	40	**12**	1.8	**0.19**	**0.0114**
13	#30	Diameter	30	40	15	1.73	0.37	0.0235
14	#30	Diameter	30	40	20	1.67	0.49	0.0363

Note: The values in bold are to highlight the performance of the optimal or most appropriate parameter for each experimental setup.

TABLE 4 Comparison results.

Setup	Density	Cutting methods	Time cost [min]	Average error [mm]	Standard deviation
8	#15	Robotic burring	1.8	**0.10**	**0.0134**
15	#15	Robotic reaming	0.5	0.12 ($p = 0.035$)	0.0239
17	#15	Conventional reaming	0.8	0.14 ($p = 0.043$)	0.0539
11	#30	Robotic burring	1.8	**0.19**	**0.0114**
16	#30	Robotic reaming	0.5	0.25 ($p = 0.004$)	0.0503
18	#30	Conventional reaming	1.2	0.26 ($p = 0.011$)	0.0617

Note: The values in bold are to highlight the performance of the optimal or most appropriate parameter for each experimental setup.

2 min. The performance is better than robotic reaming (0.12 mm, $p = 0.015$ and 0.25 mm, $p = 0.001$) and conventional reaming (0.14 mm, $p = 0.018$ and 0.26 mm, $p = 0.003$), although reaming is less time consuming (0.5 and 0.8 min, respectively). Figure 14 also shows that the proposed system has the highest accuracy and robustness. The difference in the smoothness of the hemispheres cut by these three methods are demonstrated graphically in Figure 15.

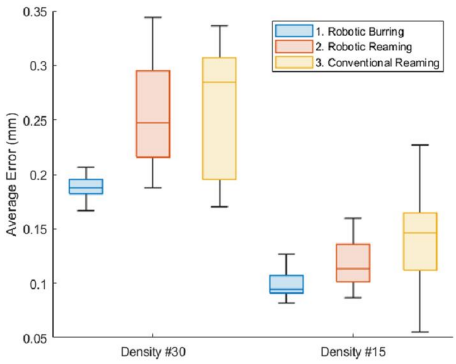

FIGURE 14 Phantom experiments comparison of robotic burring, robotic reaming, and conventional reaming.

3.2 | Cadaver experiment

The robotic burring system was also tested in a cadaver session without any significant issues (Figure 16). The Surgical and Anatomical Science Facility at University of Technology Sydney, one of Australia's foremost dedicated human anatomical laboratories, was used for the cadaver experiment. Both the robotic burring system and the robotic reaming system were tested in the cadaver experiments. Although statistically significant quantitative results were not available due to the limited number of cadaver experiments, burring results were smoother than reaming through visualisation, which is an important step towards clinical implantation.

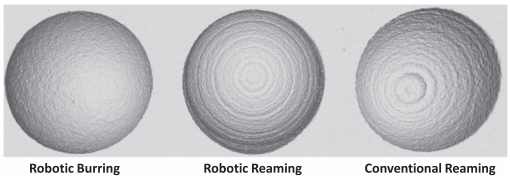

FIGURE 15 The scans of typical hemisphere examples cut by different methods.

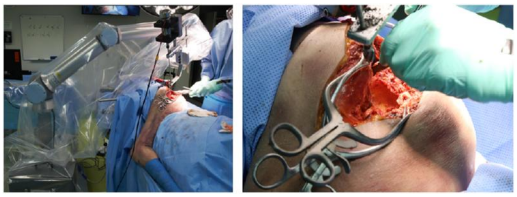

FIGURE 16 The cutting process in the cadaver experiment.

4 | DISCUSSION

The phantom experiments demonstrated that the proposed robotic burring system can produce a more accurate (Table 4) and smoother (Figure 15) surface than both robotic and conventional reaming, with consistently reduced cutting accuracy for the higher density bone blocks for all three methods. Although robotic burring is the most time consuming (1.8 vs. 0.5 min and 0.8 min for robotic burring, robotic reaming, and conventional reaming, respectively), we believe that adding approximately 1 min on an average 85 min total operating time,[31] is worth the potential benefits and therefore acceptable.

Increased accuracy of the acetabular cavity resection can result in improved press fit of the components and increased surface area contact of bone with ingrowth surfaces, increasing the speed and consistency of bone ingrowth.[6] Any unexpected shape or sizing of the reamed acetabulum can potentially lead to poor results, such as inaccurate position of the component, instability, periprosthetic fracture, or early loosening.[3,6,9] All acetabular cups have a porous surface on their back surface which grows into the bone. Therefore, the more accurate and smoother surface provides a greater contact area with the bone, and hence theoretically greater ingrowth potential thus lowering the chance of loosening which is one of the more common reasons for revision surgery. Another potential advantage of robotic-assisted burring is that it can create asymmetrical shapes by designing different trajectories such as for acetabular defects or in difficult primary hip replacements or revision cases where either a custom-made cup or augments may be required. This study has taken the first step towards clinical implantation by testing the burring in a cadaveric session without any significant issues. This system was only tested by the posterior approach[21] in the cadaver experiment, but can easily be adjusted for other hip approaches. This confirms the development of a robot burring system for hip replacement has great potential and clinical value.

There are some limitations of the current apparatus that need to be addressed. Although the current robotic burring system is relatively complete and effective, at this stage, the system cannot adjust to any potential movements of the patient during surgery. Therefore, the system is planned to be equipped with different sensors such as electromagnetic sensors,[32] which will compute the relative pose between the robot burr head and the acetabulum in real time. The information will be used as feedback such that the hemisphere can be cut accurately and safely in the event of any patient or pelvic movement. We also plan to conduct additional cadaver experiments and obtain a sufficient amount of data to further validate the performance of the system. Following this, testing the system in a clinical setting is planned.

5 | CONCLUSION

This paper presents a robotic burring system that increases the accuracy and smoothness of acetabular preparation during THR surgery. The details included mechanical design, robot trajectory optimisation, control development, and testing of the system to cut a smooth hemisphere on the bone blocks. The proposed system outperformed robotic and conventional reaming methods to produce the acetabular cavity based on phantom experiments. In the future, we plan to conduct additional cadaver experiments and test the system in a clinical setting once proper authorisation is obtained.

ACKNOWLEDGEMENTS

The authors would like to thank Kai Pan for the support of cadaver experiment. This work was supported by PMSW Research Pty Ltd, Australia.

Open access publishing facilitated by University of Technology Sydney, as part of the Wiley - University of Technology Sydney agreement via the Council of Australian University Librarians.

CONFLICT OF INTEREST STATEMENT

There are no conflicts of interest to declare.

DATA AVAILABILITY STATEMENT

The data that support the findings of this study are available on request from the corresponding author.

ORCID

Tiancheng Li https://orcid.org/0000-0003-2215-1232

REFERENCES

1. Cross M, Smith E, Hoy D, et al. The global burden of hip and knee osteoarthritis: estimates from the global burden of disease 2010 study. *Ann Rheum Dis*. 2014;73(7):1323-1330. https://doi.org/10.1136/annrheumdis-2013-204763
2. Ackerman IN, Bohensky MA, Zomer E, et al. The projected burden of primary total knee and hip replacement for osteoarthritis in Australia to the year 2030. *BMC Muscoskel Disord*. 2019;20(1):1-10. https://doi.org/10.1186/s12891-019-2411-9

3. Sloan M, Premkumar A, Sheth NP. Projected volume of primary total joint arthroplasty in the US, 2014 to 2030. *J Bone Joint Surg*. 2018;100(17):1455-1460. https://doi.org/10.2106/jbjs.17.01617
4. Tabata T, Kaku N, Hara K, Tsumura H. Initial stability of cementless acetabular cups: press-fit and screw fixation interaction—an in vitro biomechanical study. *Eur J Orthop Surg and Traumatol*. 2015;25(3):497-502. https://doi.org/10.1007/s00590-014-1571-4
5. Berahmani S, Janssen D, Kessel vS, et al. An experimental study to investigate biomechanical aspects of the initial stability of press-fit implants. *J Mech Behav Biomed Mater*. 2015;42:177-185. https://doi.org/10.1016/j.jmbbm.2014.11.014
6. Slotkin S, Frisch NB, Roc G, Silverton CD. Hemispherical and minimally invasive total hip reamers: a biomechanical analysis of use and design. *Arthroplasty today*. 2017;3(2):131-136. https://doi.org/10.1016/j.artd.2016.09.009
7. Seagrave KG, Troelsen A, Malchau H, Husted H, Gromov K. Acetabular cup position and risk of dislocation in primary total hip arthroplasty: a systematic review of the literature. *Acta Orthop*. 2017;88(1):10-17. https://doi.org/10.1080/17453674.2016.1251255
8. Feng JE, Anoushiravani AA, Eftekhary N, Wiznia D, Schwarzkopf R, Vigdorchik JM. Techniques for optimizing acetabular component positioning in total hip arthroplasty: defining a patient-specific functional safe zone. *JBJS Rev*. 2019;7(2):e5. https://doi.org/10.2106/jbjs.rvw.18.00049
9. Nd IR, Bukowski BR, Abiola R, et al. Robotic-assisted total hip arthroplasty: outcomes at minimum two-year follow-up. *Surg Technol Int*. 2017;30:365-372.
10. Hefny MS, Rudan JF, Ellis RE. Computer-assisted hip resurfacing planning using Lie group shape models. *Int J Comput Assist Radiol Surg*. 2015;10(6):707-715. https://doi.org/10.1007/s11548-015-1209-y
11. Elson L, Dounchis J, Illgen R, et al. Precision of acetabular cup placement in robotic integrated total hip arthroplasty. *Hip Int*. 2015;25(6):531-536. https://doi.org/10.5301/hipint.5000289
12. Suarez-Ahedo C, Gui C, Martin TJ, Chandrasekaran S, Lodhia P, Domb BG. Robotic-arm assisted total hip arthroplasty results in smaller acetabular cup size in relation to the femoral head size: a matched-pair controlled study. *Hip Int*. 2017;27(2):147-152. https://doi.org/10.5301/hipint.5000418
13. Lewinnek GE, Lewis J, Tarr R, Compere C, Zimmerman J. Dislocations after total hip-replacement arthroplasties. *J Bone Joint Surg Am*. 1978;60(2):217-220. https://doi.org/10.2106/00004623-197860020-00014
14. Domb BG, Redmond JM, Louis SS, et al. Accuracy of component positioning in 1980 total hip arthroplasties: a comparative analysis by surgical technique and mode of guidance. *J Arthroplasty*. 2015;30(12):2208-2218. https://doi.org/10.1016/j.arth.2015.06.059
15. Tarwala R, Dorr LD. Robotic assisted total hip arthroplasty using the MAKO platform. *Curr Rev Musculoskele Med*. 2011;4(3):151-156. https://doi.org/10.1007/s12178-011-9086-7
16. Subramanian P, Wainwright TW, Bahadori S, Middleton RG. A review of the evolution of robotic-assisted total hip arthroplasty. *Hip Int*. 2019;29(3):232-238. https://doi.org/10.1177/1120700019828286
17. Bargar WL, Bauer A, Börner M. Primary and revision total hip replacement using the Robodoc (R) system. *Clin Orthop Relat Res*. 1998;354:82-91. https://doi.org/10.1097/00003086-199809000-00011
18. Walker P, Li T, Khonasty R, et al. Proof of concept study for using UR10 robot to help total hip replacement. *Int J Med Robot Comput Assist Surg*. 2022;18(2):e2359. https://doi.org/10.1002/rcs.2359
19. Sherman WF, Flick TR, Dranoff CS, et al. Variability of cutting and thermal dynamics between new and used acetabular reamers during total hip arthroplasty. *Arthroplasty Today*. 2021;7:91-97. https://doi.org/10.1016/j.artd.2020.12.002
20. Sousa PL, Sculco PK, Mayman DJ, Jerabek SA, Ast MP, Chalmers BP. Robots in the operating room during hip and knee arthroplasty. *Curr Rev Musculoskele Med*. 2020;13(3):309-317. https://doi.org/10.1007/s12178-020-09625-z
21. Martusiewicz A, Delagrammaticas D, Harold RE, Bhatt S, Beal MD, Manning DW. Anterior versus posterior approach total hip arthroplasty: patient-reported and functional outcomes in the early postoperative period. *Hip Int*. 2020;30(6):695-702. https://doi.org/10.1177/1120700019881413
22. Walker PMS. *Method and Apparatus for Hip Replacements*. US Patent; 2017. 9,610,084.
23. Carmichael MG, Aldini S, Khonasty R, et al. The ANBOT: an intelligent robotic co-worker for industrial abrasive blasting. In: *2019 IEEE/RSJ International Conference on Intelligent Robots and Systems (IROS)*; 2019:8026-8033.
24. Kagiyama Y, Otomaru I, Takao M, et al. CT-based automated planning of acetabular cup for total hip arthroplasty (THA) based on hybrid use of two statistical atlases. *Int J Comput Assist Radiol Surg*. 2016;11(12):2253-2271. https://doi.org/10.1007/s11548-016-1428-x
25. Carmichael MG, Liu D. Admittance control scheme for implementing model-based assistance-as-needed on a robot. In: *2013 35th Annual International Conference of the IEEE Engineering in Medicine and Biology Society (EMBC)*; 2013:870-873.
26. Lynch KM, Park FC. Modern Robotics; 2017.
27. Chen Z, Wang C, Jiang W, Tang N, Chen B. A review on surgical instruments of knee arthroscopic debridement and total hip arthroplasty. *Procedia Cirp*. 2017;65:291-298. https://doi.org/10.1016/j.procir.2017.05.001
28. Calvert KL, Trumble KP, Webster TJ, Kirkpatrick LA. Characterization of commercial rigid polyurethane foams used as bone analogs for implant testing. *J Mater Sci Mater Med*. 2010;21(5):1453-1461. https://doi.org/10.1007/s10856-010-4024-6
29. Nagaraja S, Palepu V. Comparisons of anterior plate screw pullout strength between polyurethane foams and thoracolumbar cadaveric vertebrae. *J Biomech Eng*. 2016;138(10). https://doi.org/10.1115/1.4034427
30. ASTM. *Standard Specification for Rigid Polyurethane Foam for Use as a Standard Material for Testing Orthopaedic Devices and Instruments* F1839-08. ASTM International; 2021. 13.01: 6.
31. Heng Y, Gunaratne R, Ironside C, Taheri A. Conventional vs robotic arm assisted total hip arthroplasty (THA) surgical time, transfusion rates, length of stay, complications and learning curve. *J Arthritis*. 2018;7(4). https://doi.org/10.4172/2167-7921.1000272
32. Li T, Song Y, Walker P, et al. A closed-form solution to electromagnetic sensor based intraoperative limb length measurement in total hip arthroplasty. In: *International Conference on Medical Image Computing and Computer-Assisted Intervention*; 2023:365-375.

How to cite this article: Li T, Walker P, Khonasty R, et al. Robotic-assisted burring in total hip replacement: a new surgical technique to optimise acetabular preparation. *Int J Med Robot*. 2024;e2615. https://doi.org/10.1002/rcs.2615